Smart Structures and Systems, *Vol. 17, No. 3 (2016) 445-470*
DOI: http://dx.doi.org/10.12989/sss.2016.17.3.445

Investigation of modal identification and modal identifiability of a cable-stayed bridge with Bayesian framework

Sin-Chi Kuok[1a] and Ka-Veng Yuen[*2]

[1]*Department of Civil and Environmental Engineering, Cornell University, Ithaca, New York, USA 14853*
[2]*Department of Civil and Environmental Engineering, Faculty of Science and Technology, University of Macau, Macao, China*

(Received July 13, 2015, Revised October 19, 2015, Accepted December 17, 2015)

Abstract. In this study, the Bayesian probabilistic framework is investigated for modal identification and modal identifiability based on the field measurements provided in the structural health monitoring benchmark problem of an instrumented cable-stayed bridge named Ting Kau Bridge (TKB). The comprehensive structural health monitoring system on the cable-stayed TKB has been operated for more than ten years and it is recognized as one of the best test-beds with readily available field measurements. The benchmark problem of the cable-stayed bridge is established to stimulate investigations on modal identifiability and the present paper addresses this benchmark problem from the Bayesian prospective. In contrast to deterministic approaches, an appealing feature of the Bayesian approach is that not only the optimal values of the modal parameters can be obtained but also the associated estimation uncertainty can be quantified in the form of probability distribution. The uncertainty quantification provides necessary information to evaluate the reliability of parametric identification results as well as modal identifiability. Herein, the Bayesian spectral density approach is conducted for output-only modal identification and the Bayesian model class selection approach is used to evaluate the significance of different modes in modal identification. Detailed analysis on the modal identification and modal identifiability based on the measurements of the bridge will be presented. Moreover, the advantages and potentials of Bayesian probabilistic framework on structural health monitoring will be discussed.

Keywords: Bayesian inference; structural health monitoring; cable-stayed bridge; modal identification; modal identifiability

1. Introduction

Structural health monitoring of civil engineering infrastructures has received extensive attention for decades (Balageas *et al.* 2010, Brownjohn 2007, Chang *et al.* 2003, Doebling *et al.* 1996, Haldar 2013, Karbhari and Ansari 2009, Li and Ou 2011, Sohn 2004). Numerous methodologies have been proposed to accomplish various objectives of structural health monitoring. Benchmark studies on worldwide infrastructures offer open platforms for comparison among different structural health monitoring algorithms and strategies (Johnson *et al.* 2004, Ko

∗Corresponding author, Professor, E-mail: kvyuen@umac.mo
[a] Visiting Scientist, E-mail: sk2856@cornell.edu; sckuok@gmail.com

http://www.techno-press.org/?journal=sss&subpage=8 ISSN: 1738-1584 (Print), 1738-1991 (Online)

and Ni 2005, Li *et al.* 2014, Ni *et al.* 2009, Zhou *et al.* 2013).

The structural health monitoring system on a cable-stayed bridge named Ting Kau Bridge (TKB) was devised by the Highways Department of the Hong Kong SAR Government to monitor the structural integrity and performance under in-service condition. The structural response and operating condition have been monitored with more than 230 sensors including accelerometers, strain gauges, displacement transducers, anemometers, temperature sensors, GPS and weigh-in-motion sensors (Ko and Ni 2005, Ni *et al.* 2011, Wong 2004, Wong 2007). Long-term monitoring of the cable-stayed bridge has been conducted for more than ten years and the database is recognized as one of best test-beds with readily available field measurements. Based on the instrumented TKB, the structural health monitoring benchmark problem has been established for the investigation of modal identifiability (Ni *et al.* 2011). In contrast to the blooming development of output-only modal identification methods, the identifiability of the modal identification was scarcely studied so the special theme of this benchmark problem is to stimulate mechanism studies on modal identifiability. The measurements include acceleration responses acquired by the accelerometers mounted on the bridge deck and the wind conditions captured by the anemometers installed on the cable tower and bridge deck. Therefore, the modal identifiability can be investigated under different excitation conditions.

In this paper, we address this benchmark problem with the Bayesian probabilistic framework. Bayesian inference provides a rigorous framework to investigate the modal identifiability of dynamical systems (Beck 2010, Beck and Katafygiotis 1998, Box and Tiao 1973, Grigoriu 2012, Yuen 2010, Yuen and Kuok 2011) and it has been widely applied in different engineering disciplines (Au and Zhang 2012, Au *et al.* 2012a, 2012b, 2013, Chiachío *et al.* 2014, Grigoriu and Field 2008, Hoi *et al*. 2009, Li *et al.* 2004, Mu and Yuen 2015, Ng *et al.* 2015, Sohn and Law 1997, Papadimitriou *et al.* 2011, Yan *et al.* 2009, Yuen *et al.* 2013, Yuen and Kuok 2015, 2016). An appealing feature of Bayesian inference is that not only the optimal values of the modal parameters can be obtained but also the associated estimation uncertainty can be quantified in the form of probability distribution. The uncertainty quantification provides the necessary information to evaluate the reliability of the parametric identification results as well as modal identifiability. In this paper, the Bayesian spectral density approach (Katafygiotis and Yuen 2001) and the Bayesian model class selection approach (Beck and Yuen 2004) are utilized and investigated in this study. In particular, the Bayesian spectral density approach is applied for output-only modal identification. This frequency-domain approach utilizes the statistical characteristics of the discrete Fourier transform to construct the likelihood function of the modal parameters. Then, the Bayesian model class selection approach is used to evaluate the identifiability of different modes in modal identification. This approach gives the quantitative expression of the plausibility of the modal models with different number of modes. By comparing these plausibilities, the significance of different modes can be ranked. The formulation of the two applied Bayesian approaches and the detailed analysis of the cable-stayed bridge field measurement will be presented in the following sections.

2. Formulation

2.1 Bayesian spectral density approach for output-only modal identification

The Bayesian spectral density approach (Katafygiotis and Yuen 2001) is a frequency-domain

output-only modal identification approach and it can also be applied for model updating of nonlinear dynamical systems using stationary response measurements (Yuen and Beck 2003). It utilizes the statistical properties of the discrete Fourier transform to construct the likelihood function of the modal parameters. By applying the Bayesian spectral density approach on the measured structural response, the optimal modal parameters and the associated estimation uncertainty can be obtained. Successful applications on field structural health monitoring studies demonstrated the efficacy of the approach (Kuok and Yuen 2012, Kuok and Yuen 2013). The formulation of this approach is presented as follows.

Consider a linear dynamical system with N_d degrees of freedom (DOFs) and its equation of motion is given by

$$\boldsymbol{M}\ddot{\boldsymbol{x}} + \boldsymbol{C}\dot{\boldsymbol{x}} + \boldsymbol{K}\boldsymbol{x} = \boldsymbol{T}_0\boldsymbol{F} \tag{1}$$

where $\boldsymbol{M}$, $\boldsymbol{C}$ and $\boldsymbol{K}$ are the mass, damping and stiffness matrix, respectively; $\boldsymbol{T}_0$ is a force distributing matrix; and the external excitation $\boldsymbol{F}$ is modeled as zero-mean Gaussian white noise vector process with spectral intensity matrix $\boldsymbol{S}_F(\omega) = \boldsymbol{S}_{F0}$. Using modal analysis, the generalized coordinates $\boldsymbol{x}$ are transformed to the modal coordinates with $\boldsymbol{x}(t) = \boldsymbol{\Phi}\boldsymbol{q}(t)$ where $\boldsymbol{q} = \left[q_1, q_2, \dots, q_{N_d}\right]^T$ is the modal coordinate vector and $\boldsymbol{\Phi} = \left[\boldsymbol{\phi}_1, \boldsymbol{\phi}_2, \dots, \boldsymbol{\phi}_{N_d}\right]^T$ is the mode shape matrix. Therefore, the equation of motion in Eq. (1) can be uncoupled

$$\ddot{q}_r + 2\zeta_r\omega_r\dot{q}_r + \omega_r^2 q_r = f_r, \quad r = 1,2,\dots,N_d \tag{2}$$

where ω_r, ζ_r and f_r are the modal frequency, damping ratio and modal force of the r-th mode, respectively. The modal force vector $\boldsymbol{f} = \left[f_1, f_2, \dots, f_{N_d}\right]^T$ can be obtained: $\boldsymbol{f} = (\boldsymbol{M}\boldsymbol{\Phi})^{-1}\boldsymbol{T}_0\boldsymbol{F}$ so it is also a zero-mean Gaussian white noise vector process and its spectral intensity matrix is $\boldsymbol{S}_f(\omega) = \boldsymbol{S}_{f0} = (\boldsymbol{M}\boldsymbol{\Phi})^{-1}\boldsymbol{T}_0\boldsymbol{S}_{F0}\boldsymbol{T}_0^T(\boldsymbol{M}\boldsymbol{\Phi})^{-T}$.

Let Δt denote the sampling time interval and $\boldsymbol{q}(n)$ denote the discrete structural response at time the n-th time step. The measurement data set consists of N discrete time instants: $\boldsymbol{Y}_N = \{\boldsymbol{y}(n), n = 0,1,2,\dots,N-1\}$. At the n-th time step, the measurement $\boldsymbol{y}(n)$ contains N_o channels of structural response corrupted by the measurement noise $\boldsymbol{\varepsilon}$

$$\boldsymbol{y}(n) = \boldsymbol{L}_0\boldsymbol{q}(n) + \boldsymbol{\varepsilon}(n) \tag{3}$$

where $\boldsymbol{L}_0$ is the observation matrix comprised of zeros and ones to pick up the measured DOFs. The measurement noise $\boldsymbol{\varepsilon}$ is modeled as zero-mean Gaussian independent and identical distributed (i.i.d.) process with covariance matrix $\boldsymbol{\Sigma}_\varepsilon$.

The uncertain modal parameter vector to be identified is denoted as $\boldsymbol{\theta}$ and it is comprised of the structural modal parameters (i.e., modal frequencies, damping ratios and mode shape components) of the contributing modes and the characteristic parameters of the spectral intensity of the excitation and the measurement noise. To identify the uncertain modal parameter vector $\boldsymbol{\theta}$, a discrete estimator of the power spectral density matrix is utilized (Katafygiotis and Yuen 2001)

$$\boldsymbol{S}_{y,N}(\omega_k) = \frac{\Delta t}{2\pi N}\sum_{n,n'=0}^{N-1}\boldsymbol{y}(n)\boldsymbol{y}(n')^T \exp[-i\omega_k(n-n')\Delta t] \tag{4}$$

where $\omega_k = k\Delta\omega$, $k = 0,1,\dots,N_{nqy}$ with $N_{nqy} = INT(N/2)$ and $\Delta\omega = (2\pi)/(N\Delta t)$. Assume that N_s independent sets of i.i.d. time histories are available: $\boldsymbol{Y} = \left\{\boldsymbol{Y}_N^{(s)}, s = 1,2,\dots,N_s\right\}$, the corresponding spectral density matrix estimator $\boldsymbol{S}_{y,N}^{(s)}(\omega_k), s = 1,2,\dots,N_s$, can be calculated by

using Eq. (4) and the averaged spectral density estimator can be obtained by using

$$\boldsymbol{S}_{y,N}^{avg}(\omega_k) = \frac{1}{N_s}\sum_{s=1}^{N_s}\boldsymbol{S}_{y,N}^{(s)}(\omega_k) \tag{5}$$

Given that $N_s \geq N_o$, the averaged spectral density matrix estimator $\boldsymbol{S}_{y,N}^{avg}(\omega_k)$ follows the central complex N_o-variate Wishart distribution with N_s DOFs and its probability density function (PDF) is (Katafygiotis and Yuen 2001)

$$p\left(\boldsymbol{S}_{y,N}^{avg}(\omega_k)\middle|\boldsymbol{\theta},C\right) = \frac{\kappa_1\left|\boldsymbol{S}_{y,N}^{avg}(\omega_k)\right|^{N_s-N_o}}{\left|E\left[\boldsymbol{S}_{y,N}(\omega_k)|\boldsymbol{\theta},C\right]\right|^{N_s}}\exp\left(-N_s\mathrm{tr}\left\{E\left[\boldsymbol{S}_{y,N}(\omega_k)\middle|\boldsymbol{\theta},C\right]^{-1}\boldsymbol{S}_{y,N}^{avg}(\omega_k)\right\}\right) \tag{6}$$

where the constant $\kappa_1 = \pi^{-\frac{N_o(N_o-1)}{2}}N_s^{N_o(N_s-N_o)}/\prod_{s=1}^{N_s}(N_s-s)!$; $E[\cdot]$ is the mathematical expectation; $|\cdot|$ and tr$\{\cdot\}$ denote the determinant and trace of a matrix, respectively; C is the model class to specify the concerned modes. With a properly selected frequency range Ξ, the averaged spectral density estimator in $\boldsymbol{S}_{\Xi}^{avg} = \left\{\boldsymbol{S}_{y,N}^{avg}(\omega_k), \omega_k \in \Xi\right\}$ are approximately independent (Yuen *et al.* 2002) and its PDF is given by

$$p\left(\boldsymbol{S}_{\Xi}^{avg}\middle|\boldsymbol{\theta},C\right) = \prod_{\omega_k\in\Xi}p\left(\boldsymbol{S}_{y,N}^{avg}(\omega_k)\middle|\boldsymbol{\theta},C\right) \tag{7}$$

Using the Bayes' theorem, the posterior PDF of the uncertain modal parameter vector $\boldsymbol{\theta}$ is

$$p\left(\boldsymbol{\theta}|\boldsymbol{S}_{\Xi}^{avg},C\right) = \kappa_2 p(\boldsymbol{\theta}|C)p\left(\boldsymbol{S}_{\Xi}^{avg}\middle|\boldsymbol{\theta},C\right) \tag{8}$$

where κ_2 is a normalizing constant such that integrating the right hand side over the parameter space yields unity; C is the model class to be presented in Section 2.2; $p(\boldsymbol{\theta}|C)$ and $p\left(\boldsymbol{S}_{\Xi}^{avg}\middle|\boldsymbol{\theta},C\right)$ are the prior PDF and likelihood function, respectively. The prior PDF $p(\boldsymbol{\theta}|C)$ represents the prior information of the modal parameters in $\boldsymbol{\theta}$. The posterior PDF can be well approximated by a Gaussian distribution with mean $\widehat{\boldsymbol{\theta}}$ and covariance matrix $\boldsymbol{\Sigma}_{\widehat{\boldsymbol{\theta}}}$ (Box and Tiao 1973, Yuen 2010). The optimal parameter vector $\widehat{\boldsymbol{\theta}}$ can be determined by maximizing the posterior PDF. To enhance the computation condition, an objective function is defined as the negative logarithm of the posterior PDF without taking the terms that do not depend on the uncertain parameters (Katafygiotis and Yuen 2001)

$$J(\boldsymbol{\theta}) = -\ln p(\boldsymbol{\theta}|C) + N_s\sum_{\omega_k\in\Xi}\ln\left|E\left[\boldsymbol{S}_{y,N}(\omega_k)\middle|\boldsymbol{\theta},C\right]\right| + \mathrm{tr}\left\{E\left[\boldsymbol{S}_{y,N}(\omega_k)\middle|\boldsymbol{\theta},C\right]^{-1}\boldsymbol{S}_{y,N}^{avg}(\omega_k)\right\} \tag{9}$$

The optimal parameters vector $\widehat{\boldsymbol{\theta}}$ can be obtained equivalently by minimizing the objective function

$$\widehat{\boldsymbol{\theta}} = \arg\min_{\boldsymbol{\theta}} J(\boldsymbol{\theta}) \tag{10}$$

Furthermore, the covariance matrix $\boldsymbol{\Sigma}_{\widehat{\boldsymbol{\theta}}}$ can be calculated by taking the inverse of the Hessian of the objective function evaluated at $\boldsymbol{\theta} = \widehat{\boldsymbol{\theta}}$

$$\boldsymbol{\Sigma}_{\widehat{\boldsymbol{\theta}}} = \boldsymbol{H}\left(\widehat{\boldsymbol{\theta}}\right)^{-1} \tag{11}$$

where $\boldsymbol{H}\left(\widehat{\boldsymbol{\theta}}\right) \equiv \boldsymbol{\nabla}J(\boldsymbol{\theta})\boldsymbol{\nabla}^T|_{\boldsymbol{\theta}=\widehat{\boldsymbol{\theta}}}$. With the uniform prior PDF, the elements of $\boldsymbol{H}\left(\widehat{\boldsymbol{\theta}}\right)$ can be expressed as

$$H^{(r,r')}(\widehat{\boldsymbol{\theta}}) = -\frac{\partial^2 \ln p(\boldsymbol{\theta}|C)}{\partial\theta_r \partial\theta_{r'}} + N_s \left[\sum_{\omega_k \in \Xi} \frac{\partial^2}{\partial\theta_r \partial\theta_{r'}} \left\{ \ln\left|E\left[\boldsymbol{S}_{y,N}(\omega_k)|\boldsymbol{\theta}, C\right]\right| + tr\left(\left\{E\left[\boldsymbol{S}_{y,N}(\omega_k)|\boldsymbol{\theta}, C\right]^{-1} \boldsymbol{S}_{y,N}^{avg}(\omega_k)\right\}\right)\right\} \right]_{\boldsymbol{\theta}=\widehat{\boldsymbol{\theta}}} \tag{12}$$

By applying the Bayesian spectral density approach to the measured structural acceleration response, the modal parameters can be identified and the associated estimation uncertainties can be quantified.

2.2 Bayesian model class selection approach for modal identifiability

To investigate the significance of different modes on modal identification, the Bayesian model class selection approach (Beck and Yuen 2004) is utilized. This approach has been applied to various engineering problems (Chiu *et al*. 2012, Hoi *et al*. 2013, Mu *et al*. 2014, Yuen and Kuok 2010, Yuen and Mu 2015). Herein, a *model class* is referred to a *modal model* with a specified number of modes to be identified. In Bayesian model class selection, the plausibility is used as a relative measure to evaluate the modal models for modal identification. By comparing the plausibilities, the modal models can be ranked and the most plausible one can be determined. As a result, one can determine the significant modes.

Let $\{C_1, C_2, \dots, C_{N_c}\}$ denote the model class candidate set and C is a particular candidate. Using the Bayes' theorem, the plausibility of model class C is expressed as

$$P(C|D) = \frac{p(D|C)P(C)}{p(D)} \qquad C \in \{C_1, C_2, \dots, C_{N_c}\} \tag{13}$$

where D is the dynamical measurements of the underlying structure. The prior plausibilities satisfy $\sum_{j=1}^{N_c} P(C_j) = 1$. The denominator $p(D)$ is a normalizing constant such that $\sum_{j=1}^{N_c} P(C_j|D) = 1$. The factor $p(D|C)$ is called the *evidence* for the model class C provided by the data D. By taking uniform prior (i.e., $P(C) = 1/N_c$), the plausibility $P(C|D)$ is proportional to its evidence so maximizing the plausibility is equivalent to maximizing the evidence. Based on the law of total probability, the evidence $p(D|C)$ is given by

$$p(D|C) = \int_{\Theta} p(D|\boldsymbol{\theta}, C) p(\boldsymbol{\theta}|C) d\boldsymbol{\theta} \tag{14}$$

where $\boldsymbol{\theta} = \boldsymbol{\theta}(\Theta) \in \mathbb{R}^{N_\theta}$ is the parameter vector in the parameter space Θ and it represents different models in the model class C. The PDF $p(D|\boldsymbol{\theta}, C)$ is the likelihood function and $p(\boldsymbol{\theta}|C)$ is the prior PDF of the uncertain parameter vector $\boldsymbol{\theta}$ specified by the user. For globally identifiable cases (Beck and Katafygiotis 1998, Yuen 2010), the posterior PDF for $\boldsymbol{\theta}$ given a large amount of data D can be well approximated as Gaussian so the integral in Eq. (14) can be approximated by Laplace's asymptotic approximation (Beck and Yuen 2004)

$$p(D|C) \approx p(D|\widehat{\boldsymbol{\theta}}, C)\mathcal{F} \tag{15}$$

where $\widehat{\boldsymbol{\theta}}$ is the optimal parameter vector. The maximum likelihood $p(D|\widehat{\boldsymbol{\theta}}, C)$ quantifies the

data fitting performance of the model class C and it can be obtained by using the Bayesian spectral density approach. The Ockham factor $\mathcal{F}$ is a natural penalty against complicated parameterization (Beck and Yuen 2004, Gull 1988)

$$\mathcal{F} = p(\widehat{\boldsymbol{\theta}}|C)(2\pi)^{N_\theta/2}\left|\boldsymbol{H}(\widehat{\boldsymbol{\theta}})\right|^{-1/2} \tag{16}$$

where $\boldsymbol{H}(\widehat{\boldsymbol{\theta}})$ is the Hessian matrix given by Eq. (12). Consequently, the evidence of a model class represents the overall performance of data fitting capability (measured by the maximum likelihood) and the robustness of the model class (measured by the Ockham factor). By substituting the modal identification results into Eq. (15), the evidence of each model class can be obtained. Therefore, the plausibilities of the model classes can be calculated with Eq. (13). By comparing the plausibilities of all the model classes, the optimal model class is the one with the highest plausibility. The most plausible model class possesses the optimal balance between data fitting capability and robustness to modeling error (Grigoriu 2012, Yuen 2010, Zellner *et al.* 2001).

3. Application to the structural health monitoring benchmark study of Ting Kau Bridge

3.1 Background information of the monitoring system and measurement database

The layout of the Ting Kau Bridge (TKB) for this benchmark problem is shown in Fig. 1. It is a three-tower cable-stayed bridge with two main spans of 448 m and 475 m and two side spans of 127 m each. The bridge deck contains two carriageways with identical width of 18.8 m. The locations of the monitoring sensors are specified in Fig. 1. Twenty-four channels of acceleration response were measured at widely spread locations of the bridge. In particular, the accelerometers were distributed in eight deck sections. In each section, one accelerometer was placed at the central line to measure the transverse acceleration of the crossgirder and two accelerometers were placed on the two sides of the bridge deck to measure the vertical acceleration at the girders. For the wind condition, seven anemometers were installed to record the wind speed and wind direction. As shown in Fig. 1, three anemometers were mounted at the top the three towers and the other four were placed on the bridge deck.

The database of the benchmark study contains sixteen independent sets of field measurements of the TKB. The first ten sets of data contained both the acceleration response data and wind speed data. Specifically, Data Sets 1 to 6 were monitored under calm wind condition while Data Sets 7 to 10 were monitored under severe wind condition. On the other hand, Data Sets 11 to 16 are blind data containing only acceleration response data. These six data sets were captured under different wind conditions but the monitored date and time as well as the corresponding wind condition are not provided on purpose. The monitored duration of each data set was one hour. The sampling frequency of the acceleration response and the wind speed were 25.6 Hz and 2.56 Hz, respectively. Detailed descriptions about the structure, the sensing system and the monitored data sets of benchmark study can be found in (Ko and Ni 2005, Ni *et al.* 2015, Wong 2004).

According to the locations of the accelerometers (shown in Fig. 1), the acceleration measurements can be categorized into three groups: Group I refers to the measurements at locations 1, 4, 7, 10, 13, 16, 19 and 22; Group II refers to the measurements at locations 2, 5, 8, 11, 14, 17, 20 and 23; and the measurements of the remaining eight channels are categorized as Group

III. The measurements in Groups I and III are vertical response of the two sides of the bridge deck while the measurements in Group II are transverse acceleration at the central line of the bridge deck. The acceleration response histories measured at location 10 (Group I), 11 (Group II) and 12 (Group III) shown in Fig. 2. The left column corresponds to calm wind condition (Data Set 4) while the right column corresponds to severe wind condition (Data Set 7). Fig. 3 shows the standard deviation of the acceleration response and the averaged wind speed of the first ten data sets. In this figure, the three lines in the upper subplot represent the average of each group of sensors, and the two lines in the lower subplot represent the average of the three anemometers at the tower and that of the two anemometers at the bridge deck. These values are summarized in Table 1. It is found that the averaged standard deviation of the acceleration response obtained from the accelerometers in Groups I and III are almost identical while those from Group II are significantly smaller. In other words, the vertical acceleration response of the bridge decks has higher amplitude than the transverse acceleration at the central line. From the wind speed statistics in Table 1, the measurements at the towers are generally higher than the deck especially under typhoon wind loading (Data Sets 7 to 10) due to the elevation difference of the anemometers. It is observed that the amplitude of the acceleration of Data Sets 1, 3, 4, 5 and 6 are serval times higher than the others for all Groups I, II and III. It is interesting to note that these five data sets were obtained under calm wind condition, indicating that the traffic loading induces dominating effect on the response of the bridge. Under the severe wind loading, the bridge was closed and no vehicles were allowed to pass through. For Data Set 2, the measurements were obtained on a public holiday of the Lunar New Year. This reveals that the structural acceleration is more dominated by heavy traffic loading. Table 2 shows the standard deviation of the acceleration response of the six blind data sets (Data Sets 11 to 16).

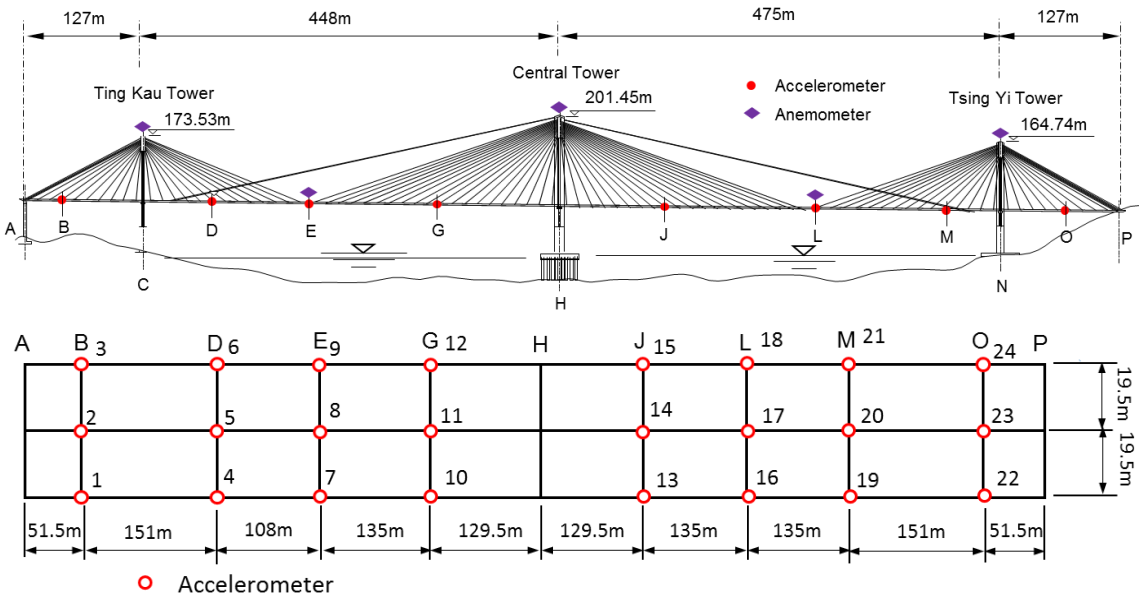

Fig. 1 Layout of Ting Kau Bridge with the locations of the monitoring sensors (provided by Ni *et al*. 2015)

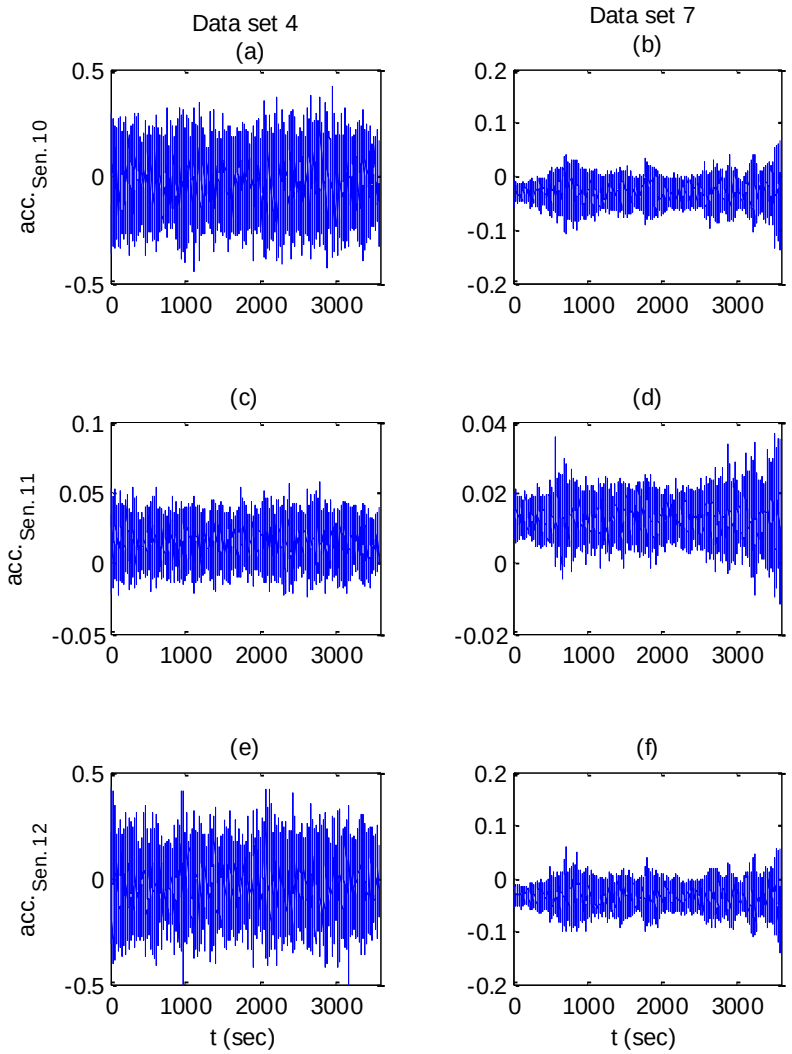

Fig. 2 Acceleration measurements of Data Sets 4 and 7 of Sensors 10, 11 and 12

Consistent with the first ten data sets, the vertical acceleration of the bridge decks (Groups I and III) were higher than the transverse acceleration at the central line (Group II). On the other hand, the amplitude of the acceleration for Data Set 15 achieved the level of other data sets monitored under calm wind condition and heavy traffic loading. However, the amplitudes of all other data sets are similar as the results obtained under the condition with limited traffic loading (Data Set 2). In the following, the modal identification results from the Bayesian spectral density approach will be presented.

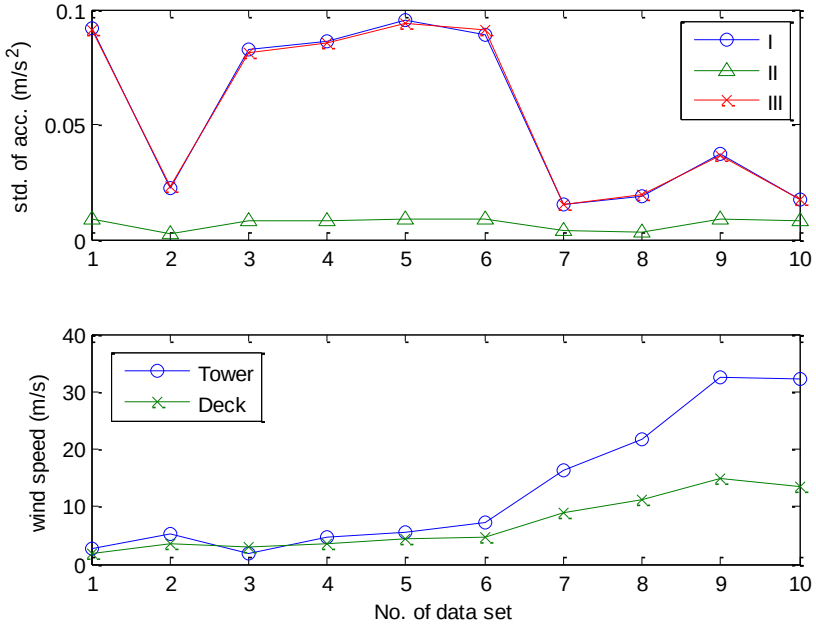

Fig. 3 Standard deviations of the acceleration response and averaged wind speed

Table 1 Statistics of the measured acceleration response and wind speed

Data Set	Monitoring Period (hh:mm-hh:mm, dd/mm/yyyy)	Standard deviation of acceleration (m/s^2)			Mean wind speed (m/s)	
		Group I	Group II	Group III	Tower	Deck
1	15:00-16:00, 28/12/1999	0.092	0.009	0.091	2.835	1.716
2	15:00-16:00, 18/02/1999	0.022	0.003	0.023	5.296	3.474
3	15:00-16:00, 01/03/1999	0.083	0.008	0.081	1.963	3.054
4	15:00-16:00, 21/06/1999	0.086	0.008	0.085	4.576	3.483
5	15:00-16:00, 24/07/1999	0.095	0.009	0.094	5.540	4.337
6	15:00-16:00, 12/08/1999	0.089	0.009	0.091	7.291	4.618
7	03:00-04:00, 07/06/1999	0.015	0.004	0.015	16.180	8.913
8	02:00-03:00, 23/08/1999	0.019	0.003	0.019	21.560	11.315
9	06:00-07:00, 16/09/1999	0.037	0.009	0.037	32.479	14.867
10	15:00-16:00, 16/09/1999	0.017	0.008	0.017	32.190	13.492

Table 2 Standard deviation of acceleration of the blind data sets

Data Set	Group I (m/s^2)	Group II (m/s^2)	Group III (m/s^2)
11	0.008	0.002	0.008
12	0.010	0.002	0.010
13	0.027	0.007	0.028
14	0.015	0.005	0.015
15	0.092	0.009	0.092
16	0.021	0.002	0.021

3.2 Modal identification with the field measurement of Ting Kau Bridge

In the following, representative results measured under different wind condition is discussed. Fig. 4 shows the response spectra of the 24-channel acceleration measurement of Data Set 4 (under calm wind condition) and Data Set 7 (under severe wind condition). The subplots on the three rows refer to the response spectra of Groups I, II and III, respectively. Since Data Sets 4 and 7 were measured in the same month (i.e., June 1999), they provide a fair ground to demonstrate the distinction of different wind conditions. The spectra demonstrate that the energy distribution varies with the monitoring location and excitation condition. Similar patterns are observed in Figs. 4a and 4e (or Figs. 4(b) and 4(f)) since the acceleration responses on the two sides of the bridge deck (Groups I and III) are highly symmetrical. For the spectra of Group II sensors, the magnitude is much lower and the energy distribution over the frequency range is substantially different from Groups I and III. Moreover, the maxima occur at the first mode (around 0.16 Hz) in Groups I and III but it occurs at the third mode (around 0.26 Hz) under the calm wind condition (Data Set 4) and at the second mode (around 0.23 Hz) under the severe wind condition (Data Set 7) in Group II. Such difference occurs because vertical accelerations were measured by Groups I and III sensors. As a result, the first mode is more pronounced. On the other hand, the transverse accelerations were measured by Group II sensors and the first mode does not have significant contribution to this direction.

The Bayesian spectral density approach is applied to the measured acceleration response for modal identification. The modal parameters of the first ten modes are identified. Note that each channel of the measurements contains significant contents of some of the ten modes only. However, by using simultaneously all channels of measurements in each group, all the ten modes can be identified. First, the identified results of the modal frequencies for Data Sets 4 and 7 are discussed. The identified values, the standard deviations and the coefficients of variation (COVs) are summarized in Table 3 and these identification results are also shown in Fig. 5 for illustration convenience. In this figure, the error bars indicate the 68% credible intervals and these intervals are sufficiently small to confirm the adequacy of measurements for modal identification. In addition, the results presented in Ni *et al.* (2015) are also shown in this figure for reference. Ni *et al.* (2015) applied the stochastic subspace identification technique to the measured 24-channel acceleration response for the identification of the modal frequencies. It can be clearly observed from Fig. 5 that the identified values of the two approaches are generally in good agreement. It is

found that except the fourth mode, the modal frequencies of the first seven modes obtained from Data Set 7 are higher than those from Data Set 4. This indicates some mild nonlinearity of the structural response and slight degradation of the structural stiffness under the severe wind condition. The standard deviations provide the estimation of the posterior uncertainty of the identified values. They are all in an acceptable range and all the COVs are less than 0.041. On the other hand, Fig. 6 shows the identified damping ratios with 68% credible intervals of Data Sets 4 and 7. Note that no published result of the damping ratios is available for comparison. By comparing with the modal frequencies, the variation of the damping ratios and hence the corresponding width of the credible intervals are much larger. This is consistent with other studies in the literature (Balageas *et al.* 2010, Brownjohn 2007, Chang *et al.* 2003, Doebling *et al.* 1996, Sohn 2004). The identified damping ratios vary between 0.4% and 5.8% and the standard deviations are in the range of 0.13% to 2.6%.

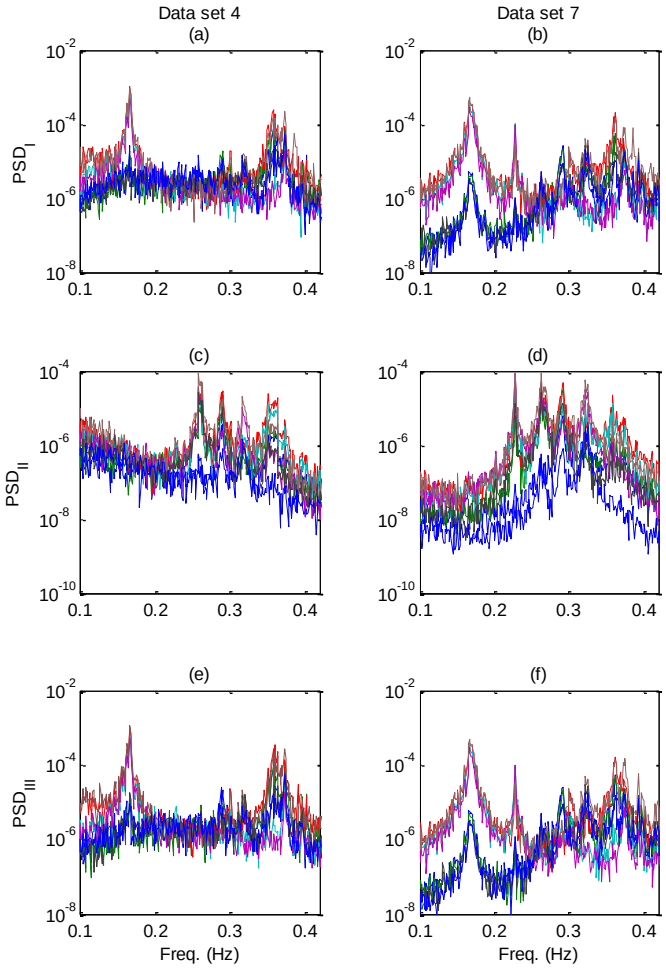

Fig. 4 Response spectra of the acceleration measurements of Data Sets 4 and 7

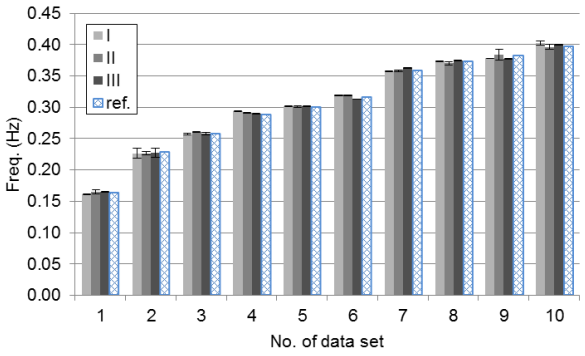

(a)

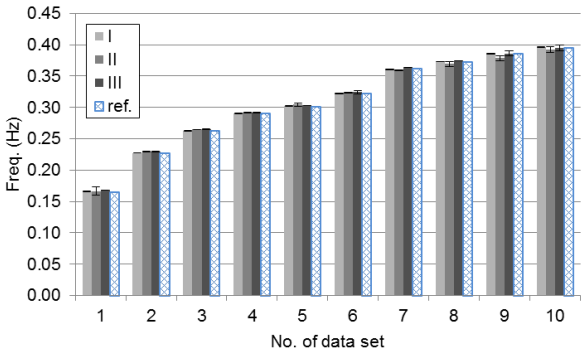

(b)

Fig. 5 Identified modal frequencies of (a) Data Set 4 and (b) Data Set 7

Table 3 Identification results of the modal frequencies

Data Set	Group	Mode / Para.	1	2	3	4	5	6	7	8	9	10
4	I	$\hat{\omega}_n$ (Hz)	0.1610	0.2267	0.2571	0.2940	0.3015	0.3188	0.3575	0.3734	0.3780	0.4022
		σ_{ω_n}(Hz)	0.0009	0.0078	0.0013	0.0007	0.0003	0.0005	0.0003	0.0005	0.0004	0.0031
		COV	0.0056	0.0344	0.0051	0.0024	0.0010	0.0016	0.0008	0.0013	0.0011	0.0077
	II	$\hat{\omega}_n$ (Hz)	0.1650	0.2265	0.2603	0.2905	0.3011	0.3185	0.3582	0.3702	0.3845	0.3965
		σ_{ω_n}(Hz)	0.0034	0.0024	0.0008	0.0006	0.0015	0.0005	0.0011	0.0022	0.0086	0.0039
		COV	0.0206	0.0106	0.0031	0.0021	0.0050	0.0016	0.0031	0.0059	0.0224	0.0098
	III	$\hat{\omega}_n$ (Hz)	0.1652	0.2275	0.2579	0.2900	0.3012	0.3130	0.3623	0.3744	0.3775	0.3997
		σ_{ω_n}(Hz)	0.0008	0.0069	0.0017	0.0005	0.0005	0.0003	0.0006	0.0003	0.0004	0.0006
		COV	0.0048	0.0303	0.0066	0.0017	0.0017	0.0010	0.0017	0.0008	0.0011	0.0015
7	I	$\hat{\omega}_n$ (Hz)	0.1659	0.2274	0.2624	0.2902	0.3021	0.3225	0.3605	0.3730	0.3854	0.3960
		σ_{ω_n}(Hz)	0.0005	0.0004	0.0007	0.0008	0.0010	0.0004	0.0008	0.0004	0.0005	0.0004
		COV	0.0030	0.0018	0.0027	0.0028	0.0033	0.0012	0.0022	0.0011	0.0013	0.0010
	II	$\hat{\omega}_n$ (Hz)	0.1667	0.2298	0.2647	0.2913	0.3044	0.3234	0.3589	0.3694	0.3785	0.3919
		σ_{ω_n}(Hz)	0.0068	0.0004	0.0004	0.0005	0.0030	0.0005	0.0009	0.0040	0.0038	0.0045
		COV	0.0408	0.0017	0.0015	0.0017	0.0099	0.0015	0.0025	0.0108	0.0100	0.0115
	III	$\hat{\omega}_n$ (Hz)	0.1682	0.2295	0.2654	0.2916	0.3031	0.3246	0.3637	0.3742	0.3860	0.3946
		σ_{ω_n}(Hz)	0.0005	0.0003	0.0007	0.0006	0.0005	0.0028	0.0004	0.0004	0.0038	0.0050
		COV	0.0030	0.0013	0.0026	0.0021	0.0016	0.0086	0.0011	0.0011	0.0098	0.0127

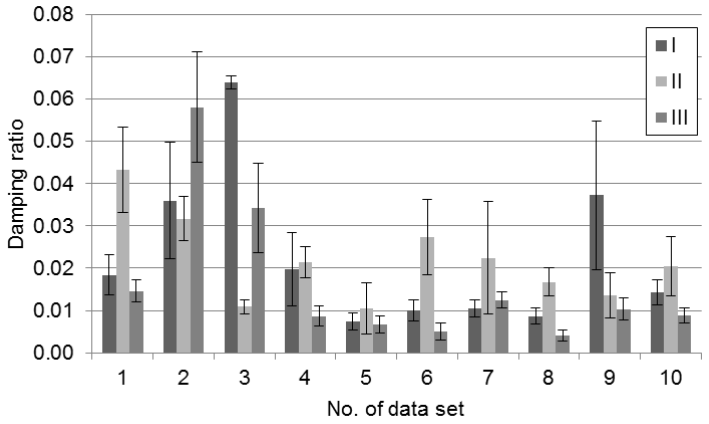

(a)

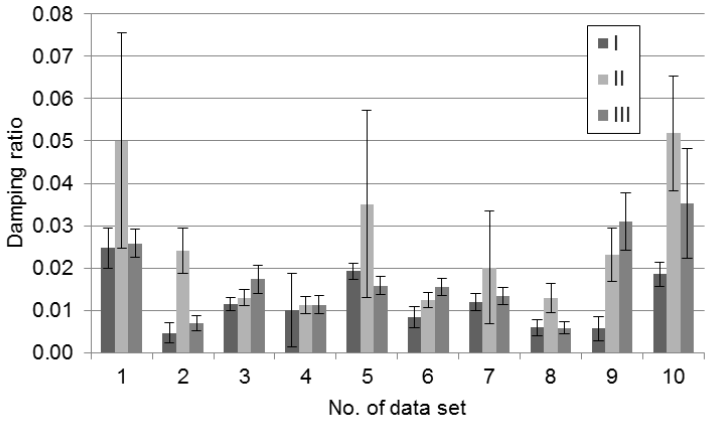

(b)

Fig. 6 Identified damping ratios of (a) Data Set 4 and (b) Data Set 7

The identified modal frequencies for all the sixteen data sets is shown in Fig. 7. The error bars again represent the 68% credible intervals. For all the three groups of sensors, the identified modal frequencies are similar. Under different monitoring conditions, the difference between the maximum and minimum of the modal frequencies is within 6.3%, 5.9% and 5.3% for Groups I, II and III, respectively. The variation trend and the estimation uncertainty of the identified modal frequencies obtained from Groups I and III are similar while the ones from Group II are different to certain extent. In Groups I and III, the identification results of the first three modes are almost identical. From the error bars, it is shown that the estimation uncertainty of the first, fifth, eighth, ninth and tenth mode in Group II is larger than that in Groups I and III. On the other hand, it is found that the estimation uncertainty of different modes changes substantially under different monitoring conditions. This is because different modes were excited under different wind conditions. For example, the error bars of the modal frequencies under severe wind condition (Data Sets 7 to 10) of the second mode are far narrower than those under calm wind condition

(Data Sets 1 to 6) because the second mode is not significant under calm wind condition. This issue will be further discussed in the next section of modal identifiability.

Fig. 8 shows the variation of the damping ratios with the 68% credible interval for the first three modes. The highest damping ratios occur in the first mode using Group II sensors and they vary between 3.7% and 9.7%. For the rest of the results, the damping ratios are in the range of 0.12% to 6.2%. It is found that that the fluctuation of the damping ratios and the estimation uncertainty are substantially larger than those of the modal frequencies. Regarding the estimation results, no statistically significant trend between the damping ratios and the monitoring conditions can be concluded. On the other hand, the large posterior uncertainty in the first mode for Data Sets 7 to 10 and the second mode for Data Sets 1 to 6 indicates the low identifiability of these mode under the corresponding wind condition. This issue will be further discussed in the next section.

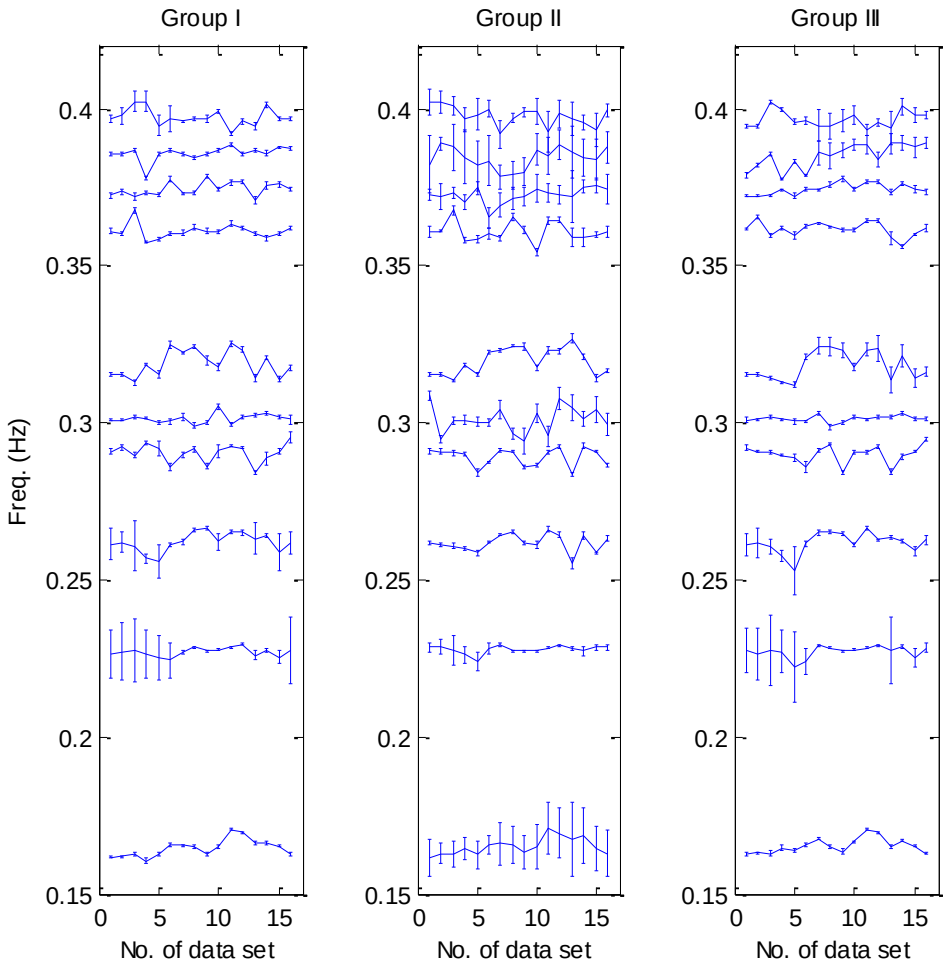

Fig. 7 Variation of the identified modal frequencies

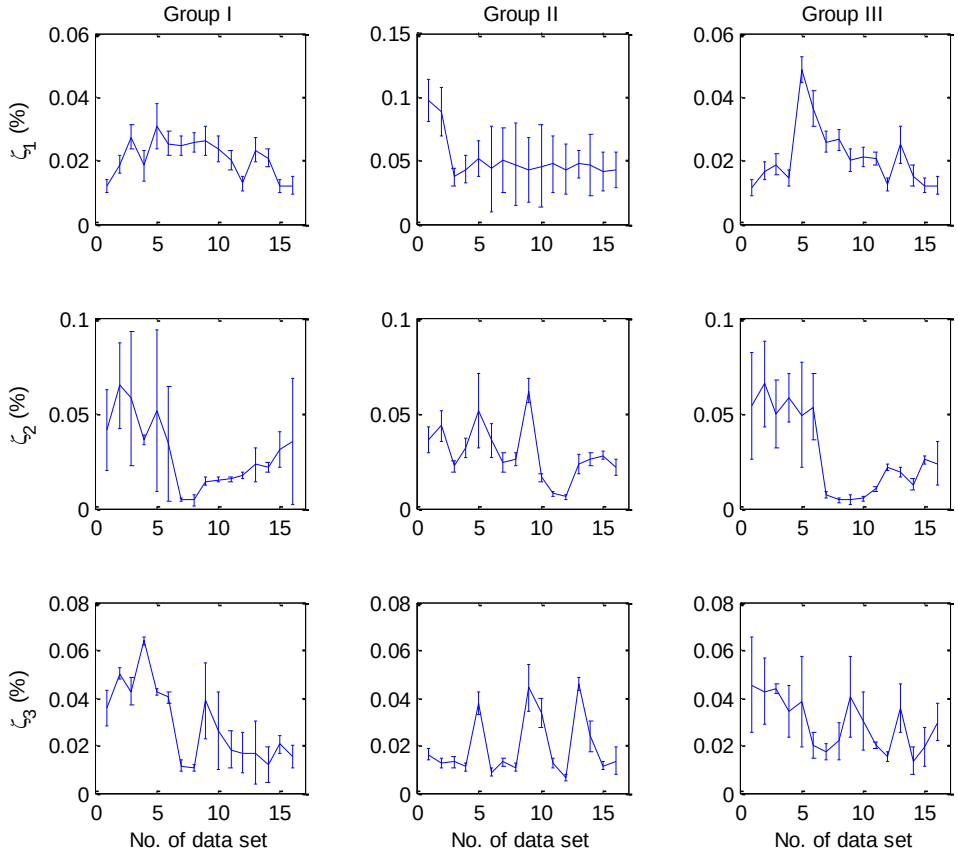

Fig. 8 Variation of the identified damping ratios

3.3 Modal identifiability under different monitoring conditions

In Section 3.2, the modal identification results were obtained by using all channels of measurements in each group of sensors and all the first ten modes could be identified. However, from the standard deviations shown in Table 3, it can be seen that the significance and identifiability vary considerably among these ten modes. If only an individual channel is used, only a few modes can be identified. In the following, Bayesian model class selection is performed to investigate this issue. A model class is referred to a modal model with a specified number of modes for identification. The modal models are evaluated using the plausibility given by Eq. (13). By comparing the plausibilities of different modal models, the optimal one can be selected so the significant modes can be determined. In this study, ten modal models, representing modal models with one to ten modes, are considered. Based on the results shown in Fig. 7, the spectra in the frequency range $[0.14, 0.41]$ Hz is used so that the frequency band covers all these ten modes.

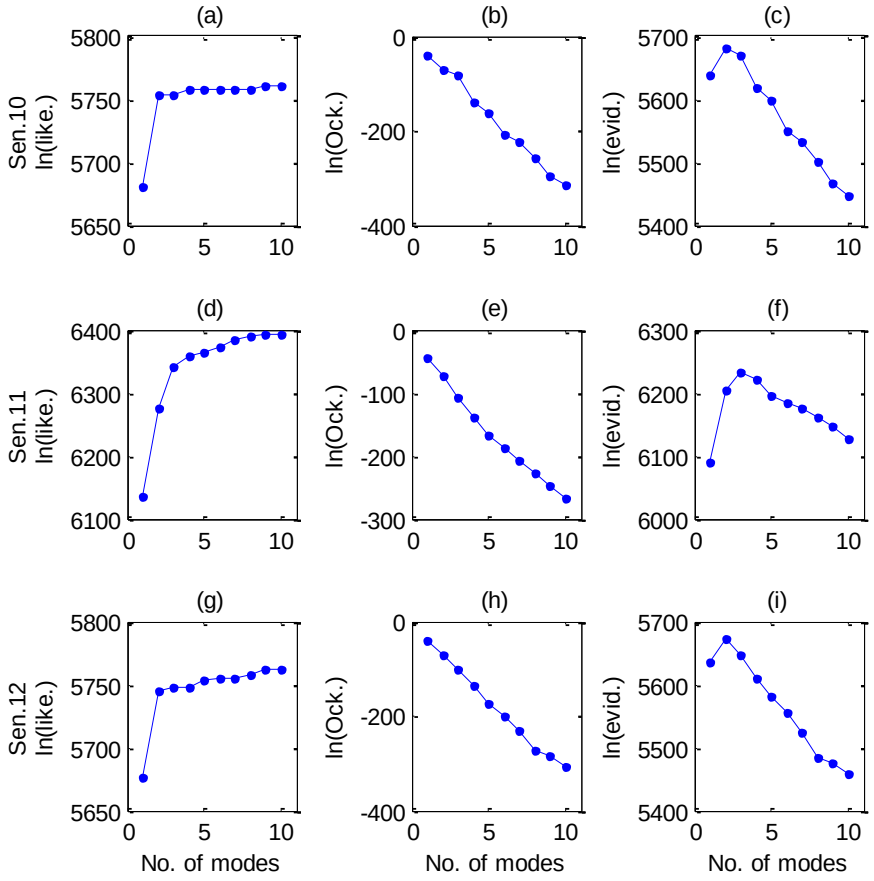

Fig. 9 Comparison of the maximum log-likelihood, log-Ockham factor and log-evidence values for different model classes of Data Set 4

First, the model selection results of Data Sets 4 and 7 are discussed. Fig. 9 shows the results of the maximum log-likelihood $\ln p(D|\hat{\boldsymbol{\theta}}, C)$, log-Ockham factor $\ln \mathcal{F}$ and log-evidence $\ln p(D|C)$ using measurements from Sensors 10, 11 and 12 of Data Set 4. As indicated in Fig. 1, the three sensors are placed near the mid-span cross section on the two sides and the central line of the bridge deck. In the same fashion as Fig. 9, Fig. 10 shows the corresponding results for Data Set 7 in the same fashion. The values of the maximum likelihood and the Ockham factor interpret the data fitting capacity and the robustness against modeling error and measurement noise, respectively. The evidence is the indicator of the overall performance of these two properties. Regarding the results of the maximum log-likelihood, notable increases occur when the number of involved modes is small and the increasing rate slows down as the number of modes increases. It is because the data fitting capacity is considerably enhanced by adding an additional mode when only limited modes are involved. However, as the number of modes increases, the improvement on

data fitting capacity saturates. On the other hand, as a penalty for the increasing complicatedness of the modal models, the log-Ockham factor decreases monotonically as the number of involved modes increases. The log-evidence is given by the sum of the maximum log-likelihood and log-Ockham factor according to Eq. (15). It is found that the performance of different modal models varies with the monitoring conditions as well as the sensor locations. For Data Set 4 (calm wind condition), the optimal modal models of Sensors 10 and 12 contains only two modes but it contains three modes for Sensor 11. For Data Set 7 (severe wind condition), more modes are involved in the optimal modal models. In particular, the optimal modal model of Sensors 10, 11 and 12 contains three, five and four modes, respectively. For both data sets, the one-mode modal model (the simplest one) obtains the lowest value in the log-evidence for Sensor 11, indicating that underfitting occurs. In contrast, the lowest value in the log-evidence for Sensors 11 and 12 refers to the ten-mode modal model (the most complicated one), indicating that overfitting occurs.

The estimated modal frequencies, plausibility and ranking of Data Sets 4 and 7 are shown in Tables 4 and 5, respectively. The modal model with ranking 1 refers to the most plausible one and the corresponding results are in italic. Note that spurious modes were identified when the number of modes is large in a modal model. For example, regarding the results of five modes with Sensor 10 in Data Set 4 (shown on the sixth row of Table 4), the identified modal frequencies $\widehat{\omega}_2 = 0.2083$ Hz and $\widehat{\omega}_4 = 0.3847$ Hz do not match the modal frequencies of the structure (shown in Fig. 7 or Table 3). In these tables, only those associated with a physical mode are bolded and the actual order of the identified mode is shown in the superscript. In all cases, the optimal modal model occupies at least 96.7% of the plausibility. Fig. 11 shows the spectra estimated from the acceleration measurements (fluctuating curves) and from the optimal modal models (smooth curves). This confirms that the optimal modal models provide sufficient yet simplest possible representation of the measured spectra. In all cases, the smooth curves match all the peaks with sufficient energy.

Next, the results of the optimal modal models for all the 24 measurement channels of Data Sets 4 and 7 are presented in Tables 6 and 7, respectively. In these tables, the belonging group of the sensor, the sensor location, the corresponding modes of the structure for the optimal modal model and the number of modes involved are listed. The corresponding modes in the optimal modal models are marked with asterisk '*'. It is observed that the optimal modal models involve more modes under the severe wind monitoring condition. It is reasonable because more apparent peaks are observed in their spectra. Under calm wind condition, the optimal modal models contain 2~4 modes. However, under severe wind condition, this number is increased to 3~6. Furthermore, in the same cross section, the optimal modal models of the two sides of the bridge deck (Groups I and III sensors) are similar but those of the central line (Group II) are different. Under calm wind condition, the second, ninth and tenth modes are not significant for any sensor and the fifth mode is significant only for Sensor 9. On the other hand, under severe wind condition, more modes were excited. Only the ninth mode is insignificant for all sensors.

Finally, the optimal modal models using measurements from Sensors 10 to 12 for all the sixteen data sets are summarized in Table 8. The most complicated optimal modal model involves only five modes and the one-mode modal model underfits the data in all cases. The first and eighth modes are significant for Sensors 10 and 12 as these two modes appear in all the optimal modal models. For the third, fourth and seventh modes, although they are not included in the optimal modal models of Sensors 10 and 12, they are included in most of the optimal modal models of Sensor 11. This is not surprising because the modal response is multiplied with the mode shape component that is location dependent. The ninth and tenth modes do not appear in any of the

optimal modal models of these three sensors. Moreover, it is found that the selection of the optimal modal models is stable under the same wind condition. For Data Sets 1 to 6 (calm wind condition), the optimal modal models of Sensors 10 and 12 are identical (involving the first and eight modes) and the optimal modal models of Sensor 11 contain two to three modes. Although the acceleration amplitude of Data Set 2 was substantially lower than others under calm wind condition (as shown in Fig. 3), the optimal modal models of Data Set 2 follow the same pattern as other data sets of calm wind condition. For Data Sets 7 to 10 (severe wind condition), the optimal modal models contain three to four modes for Sensors 10 and 12 and contain five modes for Sensor 11.

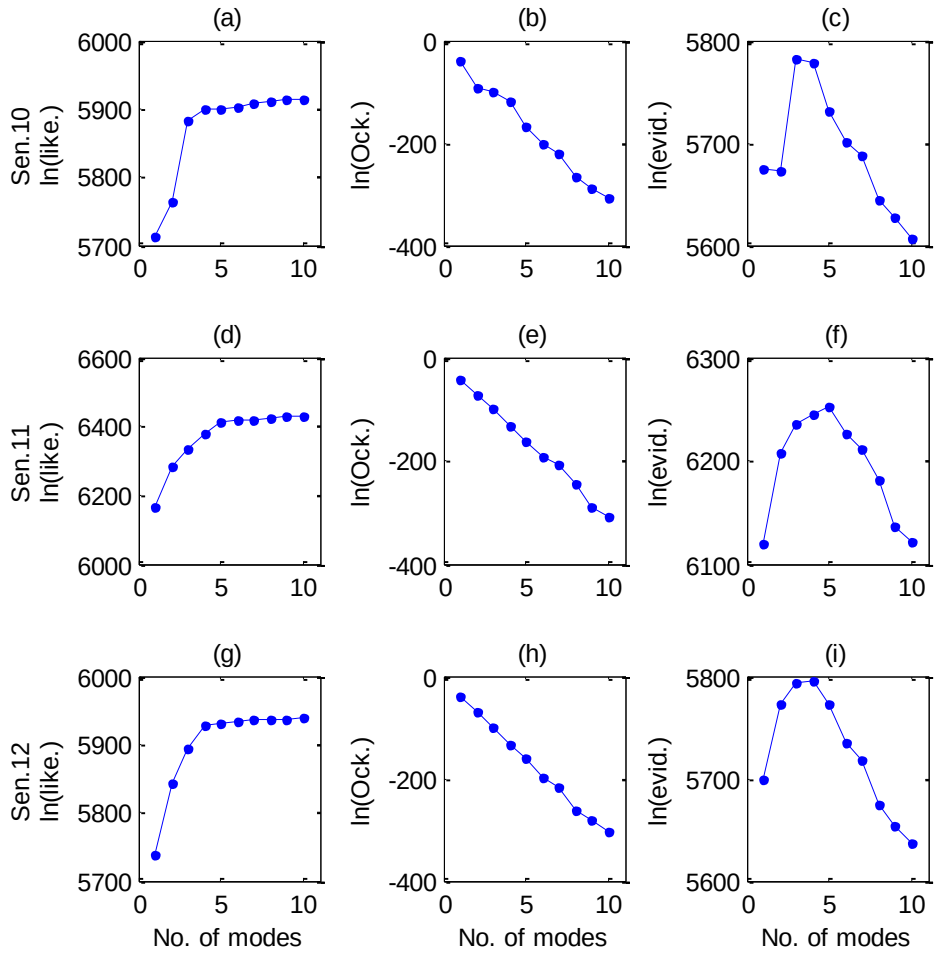

Fig. 10 Comparison of the maximum log-likelihood, log-Ockham factor and log-evidence values for different model classes of Data Set 7

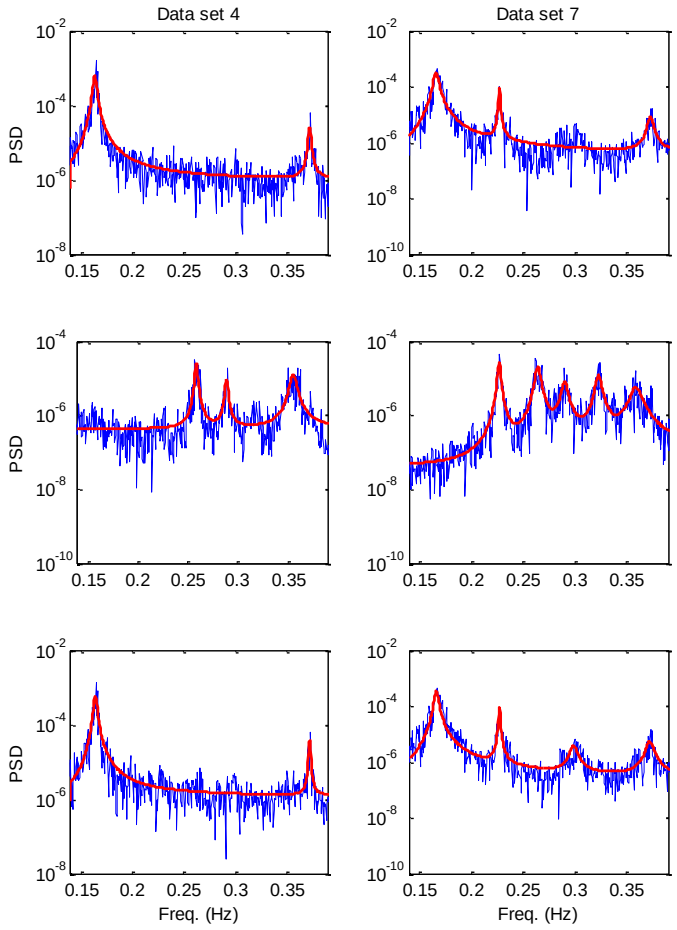

Fig. 11 Spectra estimated from acceleration measurements and from optimal models of Data Sets 4 and 7

Finally, the model class selection results provide a basis to determine the monitoring condition of the blind data sets. By comparing the results under different wind conditions, the number of significant modes in the optimal modal models for Data Sets 11 and 12 follow similar patterns as the ones under severe wind condition while the ones of Data Sets 15 and 16 are the same as those under calm wind condition. For Data Set 13, all the three optimal modal models involve two modes. For Sensors 10 and 12, the optimal modes are the same as the calm wind condition. However, Sensor 11 behaves differently and the optimal modal model contains the second and the sixth mode. According to Data Sets 1 to 10, the second mode is a common mode only under severe wind condition. For Data Set 14, although the involved modes belong to the significant modes under severe wind condition, the number of modes involved in the optimal modal models is less than those under severe wind condition given by Data Sets 7 to 10. Therefore, it is suspected that both Data Sets 13 and 14 were obtained under severe wind condition but the wind level was different from the ones associated with Data Sets 7 to 10.

Table 4 Estimated modal frequencies, plausibility and ranking for different model classes of Data Set 4

Sensor	No.of modes	$\hat{\omega}_1$ (Hz)	$\hat{\omega}_2$ (Hz)	$\hat{\omega}_3$ (Hz)	$\hat{\omega}_4$ (Hz)	$\hat{\omega}_5$ (Hz)	$\hat{\omega}_6$ (Hz)	$\hat{\omega}_7$ (Hz)	$\hat{\omega}_8$ (Hz)	$\hat{\omega}_9$ (Hz)	$\hat{\omega}_{10}$ (Hz)	Plausibility	Ranking
10	1	**0.1633**$^{(1)}$	–	–	–	–	–	–	–	–	–	2.34×10^{-19}	3
	2	***0.1631***$^{(1)}$	***0.3726***$^{(8)}$	–	–	–	–	–	–	–	–	***1.00***	***1***
	3	**0.1631**$^{(1)}$	**0.3726**$^{(8)}$	**0.4088**$^{(10)}$	–	–	–	–	–	–	–	5.79×10^{-6}	2
	4	**0.1631**$^{(1)}$	**0.2194**$^{(2)}$	**0.3605**$^{(7)}$	**0.3727**$^{(8)}$	–	–	–	–	–	–	1.11×10^{-28}	4
	5	**0.1631**$^{(1)}$	0.2083	**0.3726**$^{(8)}$	0.3847	**0.3964**$^{(10)}$	–	–	–	–	–	1.07×10^{-37}	5
	6	**0.1631**$^{(1)}$	0.2083	**0.2194**$^{(2)}$	0.2400	**0.2573**$^{(3)}$	**0.3726**$^{(8)}$	–	–	–	–	4.12×10^{-58}	6
	7	**0.1631**$^{(1)}$	0.1995	0.1995	0.2083	**0.2573**$^{(3)}$	**0.3726**$^{(8)}$	**0.4091**$^{(10)}$	–	–	–	2.43×10^{-65}	7
	8	**0.1631**$^{(1)}$	0.1995	0.2017	0.2029	0.2083	**0.2826**$^{(4)}$	**0.3726**$^{(8)}$	0.3908	–	–	6.31×10^{-80}	8
	9	**0.1631**$^{(1)}$	0.2083	**0.2194**$^{(2)}$	0.2400	0.2482	**0.3605**$^{(7)}$	**0.3727**$^{(8)}$	0.3866	**0.4036**$^{(10)}$	–	7.16×10^{-95}	9
	10	**0.1631**$^{(1)}$	0.1995	0.2083	**0.2194**$^{(2)}$	0.2362	0.2400	0.2482	**0.2845**$^{(4)}$	**0.3724**$^{(8)}$	**0.4064**$^{(10)}$	1.48×10^{-103}	10
11	1	**0.2885**$^{(4)}$	–	–	–	–	–	–	–	–	–	1.13×10^{-62}	10
	2	**0.2884**$^{(4)}$	**0.3575**$^{(7)}$	–	–	–	–	–	–	–	–	4.45×10^{-13}	3
	3	***0.2884***$^{(4)}$	***0.3575***$^{(7)}$	***0.3736***$^{(8)}$	–	–	–	–	–	–	–	***1.00***	***1***
	4	0.1434	**0.2581**$^{(3)}$	**0.2884**$^{(4)}$	**0.3575**$^{(7)}$	–	–	–	–	–	–	2.19×10^{-6}	2
	5	**0.2884**$^{(4)}$	**0.3170**$^{(6)}$	**0.3576**$^{(7)}$	0.3605	**0.4096**$^{(10)}$	–	–	–	–	–	1.21×10^{-16}	4
	6	0.1434	0.2031	0.2865	**0.2897**$^{(4)}$	**0.3170**$^{(6)}$	**0.3576**$^{(7)}$	–	–	–	–	5.93×10^{-22}	5
	7	0.1516	**0.2582**$^{(3)}$	**0.2883**$^{(4)}$	**0.3172**$^{(6)}$	**0.3538**$^{(7)}$	0.3609	**0.3735**$^{(8)}$	–	–	–	2.34×10^{-25}	6
	8	0.1513	0.2031	0.2087	**0.2581**$^{(3)}$	0.2870	**0.2898**$^{(4)}$	**0.3171**$^{(6)}$	**0.3580**$^{(7)}$	–	–	3.18×10^{-32}	7
	9	0.1507	0.1992	0.2031	0.2087	**0.2581**$^{(3)}$	**0.2883**$^{(4)}$	**0.3171**$^{(6)}$	0.3506	**0.3590**$^{(7)}$	–	1.02×10^{-38}	8
	10	0.1522	0.2031	0.2087	0.2379	**0.2581**$^{(3)}$	0.2731	0.2871	**0.2898**$^{(4)}$	**0.3171**$^{(6)}$	**0.3580**$^{(7)}$	2.11×10^{-47}	9
12	1	**0.1644**$^{(1)}$	–	–	–	–	–	–	–	–	–	3.94×10^{-17}	3
	2	***0.1643***$^{(1)}$	***0.3591***$^{(7)}$	–	–	–	–	–	–	–	–	***1.00***	***1***
	3	**0.1639**$^{(1)}$	**0.2885**$^{(4)}$	**0.3593**$^{(7)}$	–	–	–	–	–	–	–	6.72×10^{-12}	2
	4	**0.1640**$^{(1)}$	**0.2885**$^{(4)}$	**0.3567**$^{(7)}$	**0.3729**$^{(8)}$	–	–	–	–	–	–	1.62×10^{-27}	4
	5	**0.1639**$^{(1)}$	0.1977	**0.2562**$^{(3)}$	**0.2885**$^{(4)}$	**0.3594**$^{(7)}$	–	–	–	–	–	9.80×10^{-41}	5
	6	**0.1639**$^{(1)}$	**0.2245**$^{(2)}$	**0.2885**$^{(4)}$	**0.3162**$^{(6)}$	**0.3567**$^{(7)}$	**0.3729**$^{(8)}$	–	–	–	–	3.22×10^{-52}	6
	7	**0.1639**$^{(1)}$	**0.2246**$^{(2)}$	**0.2885**$^{(4)}$	**0.3162**$^{(6)}$	**0.3567**$^{(7)}$	**0.3729**$^{(8)}$	**0.3965**$^{(10)}$	–	–	–	1.17×10^{-65}	7
	8	**0.1635**$^{(1)}$	0.2099	**0.2567**$^{(3)}$	**0.2886**$^{(4)}$	**0.3167**$^{(6)}$	**0.3566**$^{(7)}$	**0.3729**$^{(8)}$	**0.4018**$^{(10)}$	–	–	3.64×10^{-82}	8
	9	**0.1635**$^{(1)}$	0.2101	**0.2566**$^{(3)}$	**0.2886**$^{(4)}$	**0.3167**$^{(6)}$	0.3500	**0.3577**$^{(7)}$	**0.3729**$^{(8)}$	**0.3965**$^{(10)}$	–	6.36×10^{-86}	9
	10	**0.1636**$^{(1)}$	0.1977	0.2171	**0.2566**$^{(3)}$	**0.2886**$^{(4)}$	**0.3167**$^{(6)}$	0.3500	**0.3577**$^{(7)}$	**0.3729**$^{(8)}$	**0.4018**$^{(10)}$	3.39×10^{-92}	10

Table 5 Estimated modal frequencies, plausibility and ranking for different model classes of Data Set 7

Sensor	No. of modes	$\hat{\omega}_1$ (Hz)	$\hat{\omega}_2$ (Hz)	$\hat{\omega}_3$ (Hz)	$\hat{\omega}_4$ (Hz)	$\hat{\omega}_5$ (Hz)	$\hat{\omega}_6$ (Hz)	$\hat{\omega}_7$ (Hz)	$\hat{\omega}_8$ (Hz)	$\hat{\omega}_9$ (Hz)	$\hat{\omega}_{10}$ (Hz)	Plausibility	Ranking
10	1	**0.1667**$^{(1)}$	–	–	–	–	–	–	–	–	–	4.78×10^{-47}	6
	2	**0.1669**$^{(1)}$	**0.3728**$^{(8)}$	–	–	–	–	–	–	–	–	1.03×10^{-47}	7
	3	***0.1662***$^{(1)}$	***0.2272***$^{(2)}$	***0.3729***$^{(8)}$	–	–	–	–	–	–	–	***9.74×10^{-1}***	***1***
	4	**0.1662**$^{(1)}$	**0.2272**$^{(2)}$	**0.3013**$^{(5)}$	**0.3730**$^{(8)}$	–	–	–	–	–	–	2.54×10^{-2}	2
	5	**0.1662**$^{(1)}$	0.2129	0.2235	**0.2272**$^{(2)}$	**0.3729**$^{(8)}$	–	–	–	–	–	2.55×10^{-22}	3
	6	**0.1662**$^{(1)}$	**0.2271**$^{(2)}$	0.2313	0.2373	**0.3729**$^{(8)}$	0.4100	–	–	–	–	2.55×10^{-35}	4
	7	**0.1662**$^{(1)}$	**0.2272**$^{(2)}$	0.2373	**0.3011**$^{(5)}$	**0.3726**$^{(8)}$	0.3900	**0.3979**$^{(10)}$	–	–	–	2.14×10^{-41}	5
	8	**0.1662**$^{(1)}$	0.2129	**0.2271**$^{(2)}$	0.2313	**0.2881**$^{(4)}$	**0.3018**$^{(5)}$	**0.3727**$^{(8)}$	**0.3977**$^{(10)}$	–	–	3.52×10^{-60}	8
	9	**0.1662**$^{(1)}$	**0.2271**$^{(2)}$	0.2313	0.2373	**0.2880**$^{(4)}$	**0.3018**$^{(5)}$	**0.3727**$^{(8)}$	**0.3799**$^{(9)}$	**0.3977**$^{(10)}$	–	5.85×10^{-68}	9
	10	**0.1662**$^{(1)}$	0.2129	0.2246	**0.2272**$^{(2)}$	0.2310	0.2373	**0.3012**$^{(5)}$	**0.3726**$^{(8)}$	0.3809	**0.3977**$^{(10)}$	1.21×10^{-76}	10
11	1	**0.2656**$^{(3)}$	–	–	–	–	–	–	–	–	–	3.16×10^{-58}	10
	2	**0.2271**$^{(2)}$	**0.2843**$^{(4)}$	–	–	–	–	–	–	–	–	7.20×10^{-20}	6
	3	**0.2270**$^{(2)}$	**0.2641**$^{(3)}$	**0.3124**$^{(6)}$	–	–	–	–	–	–	–	7.97×10^{-8}	3
	4	**0.2270**$^{(2)}$	**0.2696**$^{(3)}$	**0.3229**$^{(6)}$	**0.3587**$^{(7)}$	–	–	–	–	–	–	9.99×10^{-4}	2
	5	***0.2270***$^{(2)}$	***0.2642***$^{(3)}$	***0.2901***$^{(4)}$	***0.3228***$^{(6)}$	***0.3587***$^{(7)}$	–	–	–	–	–	***1.00***	***1***
	6	**0.2270**$^{(2)}$	**0.2642**$^{(3)}$	**0.2901**$^{(4)}$	**0.3229**$^{(6)}$	**0.3575**$^{(7)}$	**0.3734**$^{(8)}$	–	–	–	–	1.12×10^{-11}	4
	7	**0.2270**$^{(2)}$	**0.2642**$^{(3)}$	**0.2901**$^{(4)}$	**0.3229**$^{(6)}$	**0.3575**$^{(7)}$	**0.3734**$^{(8)}$	**0.3919**	–	–	–	1.80×10^{-18}	5
	8	0.2015	**0.2270**$^{(2)}$	**0.2642**$^{(3)}$	0.2841	**0.2909**$^{(4)}$	**0.3228**$^{(6)}$	**0.3575**$^{(7)}$	**0.3734**$^{(8)}$	–	–	2.81×10^{-31}	7
	9	**0.1624**$^{(1)}$	**0.2270**$^{(2)}$	**0.2642**$^{(3)}$	**0.2901**$^{(4)}$	**0.3226**$^{(6)}$	0.3375	0.3489	**0.3590**$^{(7)}$	**0.3729**$^{(8)}$	–	9.21×10^{-51}	8
	10	0.2006	**0.2271**$^{(2)}$	**0.2625**$^{(3)}$	0.2680	**0.2898**$^{(4)}$	**0.3230**$^{(6)}$	0.3489	**0.3589**$^{(7)}$	0.3693	**0.3736**$^{(8)}$	2.20×10^{-57}	9
12	1	**0.1670**$^{(1)}$	–	–	–	–	–	–	–	–	–	6.23×10^{-43}	7
	2	**0.1666**$^{(1)}$	**0.2272**$^{(2)}$	–	–	–	–	–	–	–	–	6.06×10^{-11}	3
	3	**0.1665**$^{(1)}$	**0.2272**$^{(2)}$	**0.3726**$^{(8)}$	–	–	–	–	–	–	–	3.29×10^{-2}	2
	4	***0.1665***$^{(1)}$	***0.2273***$^{(2)}$	***0.3019***$^{(5)}$	***0.3723***$^{(8)}$	–	–	–	–	–	–	***9.67×10^{-1}***	***1***
	5	**0.1665**$^{(1)}$	**0.2273**$^{(2)}$	**0.3019**$^{(5)}$	**0.3721**$^{(8)}$	**0.3951**$^{(10)}$	–	–	–	–	–	3.64×10^{-11}	4
	6	**0.1665**$^{(1)}$	0.2000	**0.2271**$^{(2)}$	0.2305	**0.3019**$^{(5)}$	**0.3723**$^{(8)}$	–	–	–	–	1.33×10^{-27}	5
	7	**0.1665**$^{(1)}$	0.2000	**0.2273**$^{(2)}$	**0.3019**$^{(5)}$	**0.3599**$^{(6)}$	**0.3728**$^{(8)}$	**0.3947**$^{(10)}$	–	–	–	7.75×10^{-35}	6
	8	**0.1665**$^{(1)}$	0.2001	**0.2272**$^{(2)}$	0.2333	0.2372	**0.3019**$^{(5)}$	**0.3722**$^{(8)}$	0.4100	–	–	4.53×10^{-54}	8
	9	**0.1665**$^{(1)}$	**0.2272**$^{(2)}$	0.2333	0.2351	0.2372	0.2864	**0.3021**$^{(5)}$	**0.3581**$^{(6)}$	**0.3726**$^{(8)}$	–	9.34×10^{-63}	9
	10	**0.1665**$^{(1)}$	**0.2271**$^{(2)}$	0.2305	0.2351	0.2372	**0.3019**$^{(5)}$	**0.3600**$^{(6)}$	**0.3727**$^{(8)}$	0.3849	**0.3949**$^{(10)}$	4.17×10^{-70}	10

Table 6 Optimal model classes for all measurement channels of Data Set 4

Group	Sensor	Mode										No. of modes
		1	2	3	4	5	6	7	8	9	10	
I	1				*			*				2
	4	*			*			*	*			4
	7	*			*			*				3
	10	*							*			2
	13	*							*			2
	16	*							*			2
	19						*		*			2
	22						*		*			2
II	2				*		*	*				3
	5			*	*			*				3
	8			*	*			*				3
	11			*	*			*				3
	14			*	*		*					3
	17			*	*		*	*				4
	20			*	*		*	*				4
	23				*		*					2
III	3	*			*			*				3
	6	*						*	*			3
	9	*				*		*				3
	12	*							*			2
	15	*							*			2
	18	*					*		*			3
	21	*					*		*			3
	24						*		*			2

Table 7 Optimal model classes for all measurement channels of Data Set 7

Group	Sensor	Mode										No. of modes
		1	2	3	4	5	6	7	8	9	10	
I	1	*		*	*		*	*			*	6
	4	*		*	*		*	*			*	6
	7	*	*					*				3
	10	*	*						*			3
	13	*	*						*			3
	16	*	*			*	*		*			5
	19	*		*	*		*		*			5
	22	*		*	*		*		*			5
II	2				*		*	*				3
	5		*	*	*			*				4
	8		*	*	*		*	*				5
	11		*	*	*		*	*				5
	14		*	*			*					3
	17		*	*	*		*					4
	20		*	*	*		*					4
	23			*	*		*					3
III	3	*		*	*		*	*				5
	6	*		*	*		*	*				5
	9	*	*			*		*				4
	12	*	*			*			*			4
	15	*	*			*			*			4
	18	*	*			*	*		*			5
	21	*		*	*		*		*			5
	24	*		*	*		*		*			5

Table 8 Optimal model classes for all data sets of Sensors 10, 11 and 12

Data Set	Sensor	Mode										No. of modes
		1	2	3	4	5	6	7	8	9	10	
	10	*							*			2
1	11			*	*			*				3
	12	*							*			2
	10	*							*			2
2	11			*	*			*				3
	12	*							*			2
	10	*							*			2
3	11			*	*			*				3
	12	*							*			2
	10	*							*			2
4	11			*	*			*				3
	12	*							*			2
	10	*							*			2
5	11			*	*			*				3
	12	*							*			2
	10	*							*			2
6	11			*			*					2
	12	*							*			2
	10	*	*						*			3
7	11		*	*	*		*	*				5
	12	*	*			*			*			4
	10	*	*			*			*			4
8	11		*	*	*		*		*			5
	12	*	*			*			*			4
	10	*	*			*			*			4
9	11		*	*	*		*	*				5
	12	*	*			*			*			4
	10	*	*			*			*			4
10	11		*	*	*		*	*				5
	12	*	*						*			3
	10	*	*			*			*			4
11	11		*	*	*		*	*				5
	12	*	*			*			*			4
	10	*	*			*			*			4
12	11		*	*	*		*	*				5
	12	*	*			*			*			4
	10	*							*			2
13	11		*				*					2
	12	*							*			2
	10	*	*						*			3
14	11		*	*			*					3
	12	*	*						*			3
	10	*							*			2
15	11			*	*			*				3
	12	*							*			2
	10	*							*			2
16	11			*	*			*				3
	12	*							*			2

In this section, the results of modal identification and modal identifiability of TKB obtained under different monitoring conditions were presented. The modal identification was conducted by applying the Bayesian spectral density approach, and hence the estimated modal parameters as

well as the associated estimation uncertainties were determined. The results demonstrated that the monitoring condition induces considerable effects not only on the modal parameters but also the modal identifiability. To further understand the modal identifiability, the Bayesian model class selection approach was applied to evaluate the plausibilities of different modal models. By comparing their plausibilities, the performance of the modal models was ranked and the optimal one was determined. This revealed that the credibility of the identified modes depends on the monitoring conditions and the optimal model modal under calm or severe wind condition was different. Such information provides a reference to decide the monitoring wind condition of the blind data sets. In contrast to deterministic approaches, Bayesian probabilistic approaches can provide the optimal estimation as well as quantify the associated estimation uncertainty. The estimated uncertainty indicates the reliability of the estimation and offers a distinct basis for investigating the modal identifiability in contrast to deterministic approaches. This paper showed that the Bayesian framework can successfully achieve the goal of the TKB benchmark study.

4. Conclusions

This paper addresses the structural health monitoring benchmark problem of the Ting Kau Bridge (TKB) using the Bayesian probabilistic framework. In particular, the Bayesian spectral density approach is used for output-only modal identification and the Bayesian model class selection approach is utilized to investigate the modal identifiability. Taking the advantage of Bayesian inference, the optimal modal parameters can be identified as well as the associated estimation uncertainty can be quantified. The identification results of the modal frequencies and damping ratios under various monitoring conditions were presented. Moreover, the effects of the sensor locations and the monitoring conditions on the performance of modal identification were discussed. The modal identifiability analysis demonstrated the importance of proper selection on the significant modes for identification. The results revealed that the credibility of the identified modes depends on the monitoring conditions. Therefore, they can be served as a basis to determine the monitoring condition of the blind data sets. The benchmark study on TKB provides a valuable platform for structural health monitoring of bridges and this study demonstrated the efficacy and potential of Bayesian inference on structural health monitoring.

Acknowledgments

This work was supported by the Science and Technology Development Fund of the Macau SAR government under Research Grant No. 012/2013/A1. This generous support is gratefully acknowledged.

References

Au, S.K. and Zhang, F.L. (2012), "Ambient modal identification of a primary-secondary structure by Fast Bayesian FFT method", *Mech. Syst. Signal Pr.*, **28**, 280-296.

Au, S.K., Ni, Y.C., Zhang, F.L. and Lam, H.F. (2012a), "Full-scale dynamic testing and modal idnetification of a coupled floor slab system", *Eng. Struct.*, **37**, 167-178.

Au, S.K., Zhang, F.L. and Ni, Y.C. (2013), "Bayesian operational modal analysis: Theory, computation, practice", *Comput. Struct.*, **126**, 3-14.
Au, S.K., Zhang, F.L. and To, P. (2012b), "Field observations on modal properties of two tall buildings under strong wind", *J. Wind Eng. Ind. Aerod.*, **101**, 12-23.
Balageas, D., Fritzen, C.P. and Güemes, A. (2010), *Structural Health Monitoring*: Wiley.
Beck, J.L. (2010), "Bayesian system identification based on probability logic", *Struct. Control. Health.*, **17**(7), 825-847.
Beck, J.L. and Katafygiotis, L.S. (1998), "Updating models and their uncertainties. I: Bayesian statistical framework", *J. Eng. Mech. - ASCE*, **124**(4), 455-461.
Beck, J.L. and Yuen, K.V. (2004), "Model selection using response measurements: Bayesian probabilistic approach", *J. Eng. Mech. - ASCE*, **130**(2), 192-203.
Box, G.E.P. and Tiao, G.C. (1973), *Bayesian Inference in Statistical Analysis*, Reading, Mass.,: Addison-Wesley Pub. Co.
Brownjohn, J.M.W. (2007), "Structural health monitoring of civil infrastructure", *Philos. T. R. Soc. A,*, **365**(1851), 589-622.
Chang, P.C., Flatau, A. and Liu, S.C. (2003), "Review paper: health monitoring of civil infrastructure", *Struct. Health. Monit.*, ***2***(3), 257-267.
Chiachío, M., Chiachío, J., Rus, G. and Beck, J.L. (2014), "Predicting fatigue damage in composites: A Bayesian framework", *Struct. Saf.*, ***51***, 57-68.
Chiu, C.F., Yan, W.M. and Yuen, K.V. (2012), "Reliability analysis of soil-water characteristics curve and its application to slope stability analysis", *Eng. Geol.*, **135**, 83-91.
Doebling, S.W., Farrar, C.R., Prime, M.B. and Shevitz, D.W. (1996), *Damage identification and health monitoring of structural and mechanical systems from changes in their vibration characteristics: A literature review, No. LA--13070-MS*, Los Alamos National Lab., NM.
Grigoriu, M. (2012), *Stochastic Systems: Uncertainty Quantification and Propagation*, Springer Science & Business Media.
Grigoriu, M. and Field, R. (2008), "A solution to the static frame validation challenge problem using Bayesian model selection", *Comput. Method Appl. M.*, **197**(29), 2540-2549.
Gull, S.F. (1988), *Bayesian inductive inference and maximum entropy*, In *Maximum-Entropy and Bayesian Methods in Science and Engineering*, Springer Netherlands.
Haldar, A. (2013), *Health Assessment of Engineered Structures: Ridges, Buildings and Other Infrastructures*, World Scientific Publishing Company Incorporated.
Hoi, K.I., Yuen, K.V. and Mok, K.M. (2009), "Prediction of daily averaged PM10 concentrations by statistical time-varying model", *Atmos. Environ.*, **43**(16), 2579-2581.
Hoi, K.I., Yuen, K.V. and Mok, K.M. (2013),"Improvement of the multilayer perceptron for air quality modelling through an adaptive learning scheme", *Comput. Genosci.*, **59**, 148-155.
Johnson, E., Lam, H., Katafygiotis, L. and Beck, J. (2004), "Phase I IASC-ASCE structural health monitoring benchmark problem using simulated data", *J. Eng. Mech. - ASCE*, **130**(1), 3-15.
Karbhari, V.M. and Ansari, F. (2009), *Structural Health Monitoring of Civil Infrastructure Systems*, Elsevier Science.
Katafygiotis, L.S. and Yuen, K.V. (2001), "Bayesian spectral density approach for modal updating using ambient data", *Earthq. Eng. Struct. D.*, ***30***(8), 1103-1123.
Ko, J. and Ni, Y. (2005), "Technology developments in structural health monitoring of large-scale bridges", *Eng. Struct.*, **27**(12), 1715-1725.
Kuok, S.C. and Yuen, K.V. (2012), "Structural health monitoring of Canton Tower using Bayesian framework", *Smart Struct. Syst.*, **10**(4-5), 375-391.
Kuok, S.C. and Yuen, K.V. (2013), "Structural health monitoring of a reinforced concrete building during the severe typhoon Vicente in 2012", *Sci. World. J.*, Article ID 509350.
Li, H. and Ou, J. (2011), "Structural health monitoring: From sensing technology stepping to health diagnosis", *Procedia Eng.*, **14**, 753-760.
Li, S., Li, H., Liu, Y., Lan, C., Zhou, W. and Ou, J. (2014), "SMC structural health monitoring benchmark

problem using monitored data from an actual cable-stayed bridge", *Struct. Control. Hlth*., **21**(2), 156-172.
Li, S., Suzuki, Y. and Noori, M. (2004), "Improvement of parameter estimation for non-linear hysteretic systems with slip by a fast Bayesian bootstrap filter", *Int. J. Nonlin. Mech*., **39**(9), 1435-1445.
Mu, H.Q., Xu, R.R. and Yuen, K.V. (2014), "Seismic attenuation relationship with homogeneous and heterogeneous prediction-error variance models", *Earthq. Eng. Eng. Vib*., **13**(1), 1-11.
Mu, H.Q. and Yuen, K.V. (2015), "Novel outlier-resistant extended Kalman filter for robust online structural identification", *J. Eng. Mech.- ASCE* , **141**(1), doi: 10.1061/(ASCE)EM.1943-7889.0000810.
Ng, I.T., Yuen, K.V. and Dong, L. (2015), "Probabilistic real-time updating for geotechnical properties evaluation", *Struct. Eng. Mech*., **54**(2), 363-378.
Ni, Y., Wang, Y. and Xia, Y. (2015), "Investigation of mode identifiability of a cable-stayed bridge: comparison from ambient vibration responses and from typhoon-induced dynamic responses", *Smart Struct. Syst*., **15**(2), 447-468.
Ni, Y., Wong, K. and Xia, Y. (2011), "Health checks through landmark bridges to sky-high structures", *Adv. Struct. Eng*., **14**(1), 103-119.
Ni, Y., Xia, Y., Liao, W. and Ko, J. (2009), "Technology innovation in developing the structural health monitoring system for Guangzhou New TV Tower", *Struct. Control. Health*., **16**(1), 73-98.
Papadimitriou, C., Fritzen, C. P., Kraemer, P. and Ntotsios, E. (2011), "Fatigue predictions in entire body of metallic structures from a limited number of vibration sensors using Kalman filtering", *Struct. Control. Health.*, **18**(5), 554-573.
Sohn, H. (2004), *A Review of Structural Health Monitoring Literature: 1996-2001*, Los Alamos National Laboratory.
Sohn, H. and Law, K.H. (1997), "A Bayesian probabilistic approach for structure damage detection", *Earthq. Eng. Struct. D*., **26**(12), 1259-1281.
Wong, K.Y. (2004), "Instrumentation and health monitoring of cable-supported bridges", *Struct. Control. Health*., **11**(2), 91-124.
Wong, K.Y. (2007), "Design of a structural health monitoring system for long-span bridges", *Struct. Infrastruct. E*., **3**(2), 169-185.
Yan, W.M., Yuen, K.V. and Yoon, G.L. (2009), "Bayesian probabilistic approach for the correlations of compression index for marine clays", *J. Geotech. Geoenviron*., **135**(12), 1932-1940.
Yuen, K.V. (2010), *Bayesian Methods for Structural Dynamics and Civil Engineering*, John Wiley & Sons, Singapore, Hoboken, NJ.
Yuen, K.V. and Beck, J.L. (2003), "Updating properties of nonlinear dynamical systems with uncertain input", *J. Eng. Mech. - ASCE*, **129**(1), 9-20.
Yuen, K.V., Katafygiotis, L.S. and Beck, J.L. (2002), "Spectral density estimation of stochastic vector processes", *Probabilist. Eng. Mech.*, **17**(3), 265-272.
Yuen, K.V. and Kuok, S.C. (2010), "Modeling of environmental influence in structural health assessment for reinforced concrete buildings", *Earthq. Eng. Eng. Vib*., **9**(2), 295-306.
Yuen, K.V. and Kuok, S.C. (2011), "Bayesian methods for updating dynamic models", *Appl. Mech. Rev*., **64**(1), Article number 010802.
Yuen, K.V. and Kuok, S.C. (2015), "Efficient Bayesian sensor placement algorithm for structural identification: a general approach for multi-type sensory systems", *Earthq. Eng. Struct. D*., **44**(5), 757-774.
Yuen, K.V. and Kuok, S.C. (2016), "Online updating and uncertainty quantification using nonstationary output-only measurement", *Mech. Syst. Signal Pr*., **66-67**, 62-77.
Yuen, K.V., Liang, P.F. and Kuok, S.C. (2013), "Online estimation of noise parameters for Kalman filter", *Struct. Eng. Mech*., **47**(3), 361-381.
Yuen, K.V. and Mu, H.Q. (2015), "Real-time system identification: an algorithm for simultaneous model class selection and parametric identification", *Comput.-Aided Civ. Inf.*, **30**(10), 785-801.
Zellner, A., Keuzenkamp, H.A. and McAleer, M. (2001), *Simplicity, Inference and Modelling: Keeping it Sophisticatedly Simple*, Cambridge University Press.

Zhou, L., Yan, G., Wang, L. and Ou, J. (2013), "Review of benchmark studies and guidelines for structural health monitoring", *Adv. Struct. Eng.*, **16**(7), 1187-1206.